Structure of a single particle from scattering by many particles randomly oriented about an axis: toward structure solution without crystallization?

2010 New J. Phys. 12 035014

(http://iopscience.iop.org/1367-2630/12/3/035014)

New Journal of Physics
The open-access journal for physics

Structure of a single particle from scattering by many particles randomly oriented about an axis: toward structure solution without crystallization?

D K Saldin[1,7], V L Shneerson[1], M R Howells[2], S Marchesini[2], H N Chapman[3], M Bogan[4], D Shapiro[2,5], R A Kirian[6], U Weierstall[6], K E Schmidt[6] and J C H Spence[6]

[1] Department of Physics, University of Wisconsin-Milwaukee, Milwaukee, WI 53211, USA
[2] Lawrence Berkeley National Laboratory, Berkeley, CA 94720, USA
[3] Center for Free Electron Laser Science, DESY, and Universität Hamburg, 22607 Hamburg, Germany
[4] SLAC National Accelerator Laboratory, 2575 Sand Hill Road, Menlo Park, CA 94025, USA
[5] Brookhaven National Laboratory, Upton, NY 11973, USA
[6] Department of Physics, Arizona State University, Tempe, AZ 82851, USA
E-mail: dksaldin@uwm.edu

New Journal of Physics **12** (2010) 035014 (14pp)
Received 1 October 2009
Published 31 March 2010
Online at http://www.njp.org/
doi:10.1088/1367-2630/12/3/035014

Abstract. In this paper is demonstrated a complete algorithm for determining the electron density of an individual particle from diffraction patterns of many particles, randomly oriented about a single axis. The algorithm operates on angular correlations among the measured intensity distributions. We also demonstrate the ability to recover the angular correlation functions of a single particle from measured diffraction patterns.

[7] Author to whom any correspondence should be addressed.

Contents

1. Introduction

The reconstruction of a high-resolution image of a single particle from scattering by several symmetrically equivalent ones has been demonstrated recently [1]. We present here a solution to the more general case of scattering by many particles, randomly oriented about an axis. The sustained x-ray or electron fluence needed for image reconstruction would destroy all high-resolution detail if focused on a single molecule, since resolution varies inversely as the third or fourth power of fluence [2]. By sharing this fluence over many identical molecules, crystallography both amplifies the scattered intensities and allows reconstruction of the periodically averaged undamaged charge density of a molecule. Part of the price for this crystallographic redundancy is that the scattered signal is sampled only at the Shannon 'frequency' of the complex *amplitudes*, resulting in loss of phase information. If the scattered *intensities* from a single molecule could be measured at their (finer) Shannon angular sampling rate, the structure of the scatterer could be determined by iterative phasing algorithms [3]. These advantages of signal amplification, damage reduction for high resolution and access to oversampled intensities (allowing solution of the phase problem) may be combined if the structure of a single particle may be determined from diffraction patterns from many identical particles in random orientations. This is possible if scattering is recorded either from stationary particles or for a recording time less than the rotational diffusion time.

Consider x-ray scattering from identical molecules in solution. If the scattering is from radiation of pulse lengths longer than the rotational diffusion time, τ, of the molecules, the signal from each molecule will be its rotational average and signal amplification is provided by the addition of such rotational averages from all illuminated molecules, as exploited by the technique of small-angle x-ray scattering (SAXS). Although it was initially thought that only angularly averaged quantities such as the average size and radius of gyration may be extracted from an angularly averaged $I(q)$ curve, it has been demonstrated [4, 5] that, with

some reasonable additional assumptions, even anisotropic details of the molecular shape may be found from measured SAXS data. Nevertheless, variations in a SAXS signal are greatest in the region of very small magnitude scattering wave vector, q, where the signal is sensitive largely to the overall shape of the molecule, rather than its internal structure [6].

The increasing availability of intense short-pulse x-ray sources allows measurements of a type not possible before, namely fluctuations of intensity about mean SAXS values from instantaneous snapshots of a relatively small number of identical particles, differing only in random position and random orientation. This becomes possible with intense radiation pulses shorter than τ. The resulting instantaneous diffraction patterns will contain intensities that are not quite constant on rings of constant q. The angular correlation functions of these intensity fluctuations contain information about the diffraction volume of the individual scatterers [7, 8]. More intense x-ray sources also allow a useful signal to be measured from higher values of q, thus permitting access to higher resolution structure. Completely new possibilities for structure determination of individual non-crystallized molecules become possible if such single-particle diffraction volumes may be deduced reliably.

Although this idea may be applied to e.g. completely randomly oriented molecules in a liquid [7], we examine here a case where the orientations of the individual particles are assumed random only about a single axis parallel to the incident beam (or perpendicular to the plane of the diffraction pattern, if a flat Ewald sphere is assumed). A possible application of this geometry is for the structure determination of e.g. a membrane-bound protein *in situ* with the membrane perpendicular to the incident beam, where the individual proteins may be assumed identical in structure, but randomly oriented about an axis perpendicular to the membrane. This is a reasonable model of e.g. K-channel proteins [9] embedded in membrane, since their function depends on the presence of a pore (the K-channel) that joins the interior of a cell to its outside.

2. Diffraction pattern from a rod with the axis perpendicular to an incident x-ray beam

We illustrate the principle with an artificial object consisting of a right cylinder of uniform refractive index n, radius a, length d and director, i.e. axis, $\mathbf{d}$. Under the Born approximation, the differential scattering cross section is

$$\frac{\mathrm{d}\sigma}{\mathrm{d}\Omega} = \frac{\omega^4 a^2}{c^4} \frac{|n^2-1|^2}{(\mathbf{q}\cdot\hat{\mathbf{d}})^2[q^2-(\mathbf{q}\cdot\hat{\mathbf{d}})^2]}(1-\sin^2\theta\cos^2\phi)\sin^2\left(\frac{\mathbf{q}\cdot\mathbf{d}}{2}\right)J_1^2(a\sqrt{q^2-(\mathbf{q}\cdot\mathbf{d})^2}). \tag{1}$$

The beam was assumed incident along the $\hat{z}$-axis, with $\mathbf{q} = \frac{\omega}{c}[\sin\theta\cos\phi\hat{x} + \sin\theta\sin\phi\hat{y} + (\cos\theta - 1)\hat{z}]$, where θ and ϕ are the polar and azimuthal angles of scattering, and incident polarization along the $\hat{x}$-axis. The polarization term $1-\sin^2\theta\cos^2\phi$ was summed over the two orthogonal polarizations of the far-field diffracted wave. Although, on our simple model, a typical membrane protein may be better approximated with $\mathbf{d}$ parallel to $\hat{z}$, for this simplified object, our principle is better illustrated with this axis taken in the $\hat{x}$–$\hat{y}$ plane. If such a cylinder is assumed to have its director $\mathbf{d}$ along the y-axis, its projection onto a plane perpendicular to the incident beam will be a rectangle with the longer side parallel to the y-axis. The x-ray diffraction pattern from such an object would be expected to be a superposition of mutually perpendicular sinc functions, giving rise to sets of fringes parallel to the x- and y-axes around a central high-intensity region. This is precisely what is seen in the calculated diffraction pattern

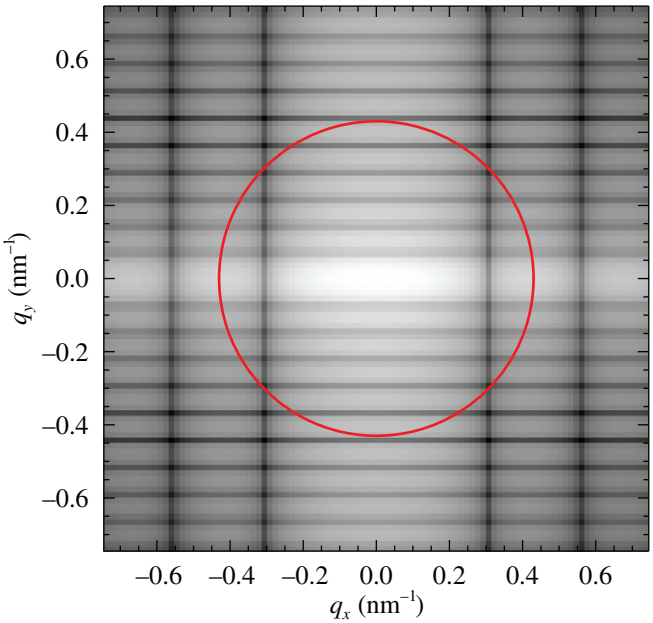

Figure 1. Simulated diffraction pattern from a single rod, whose axis is aligned parallel to the q_y-axis of the figure. The red circle marks the resolution to which this pattern will be reconstructed from 100 diffraction patterns of randomly oriented particles like that of figure 2.

of figure 1. Note the particularly high-intensity band through the center of the diffraction pattern and parallel to the q_x-axis.

3. Diffraction pattern from many rods, randomly oriented about an axis perpendicular to the diffraction pattern

We next simulate a diffraction pattern resulting from x-rays incident on ten such identical rods, related only by random orientations about an axis perpendicular to the diffraction pattern.

The pattern (figure 2) is clearly a superposition of diffraction patterns of the form of figure 1 with ten bright horizontal central bands as seen in that figure randomly oriented about the center of the pattern. In this paper, we investigate whether it is possible to develop an algorithm for recovering the single-particle diffraction pattern of figure 1 from many short-pulse multi-particle diffraction patterns of the form of figure 2 representing instantaneous positions of rods, randomly oriented about the z-axis.

Although we have performed our simulations for ten particles per diffraction pattern, essentially the same results are obtained for any (relatively small) number of particles. The only practical concern is that measurements of the angular fluctuations about the mean SAXS value on a particular resolution ring q are easier for a relatively small number of particles per diffraction pattern. However, to obtain convergent values for the correlations, it is necessary to average them over a relatively large number of diffraction patterns (100 in the case of our simulations). The experimental results of section 8 bear out these conclusions.

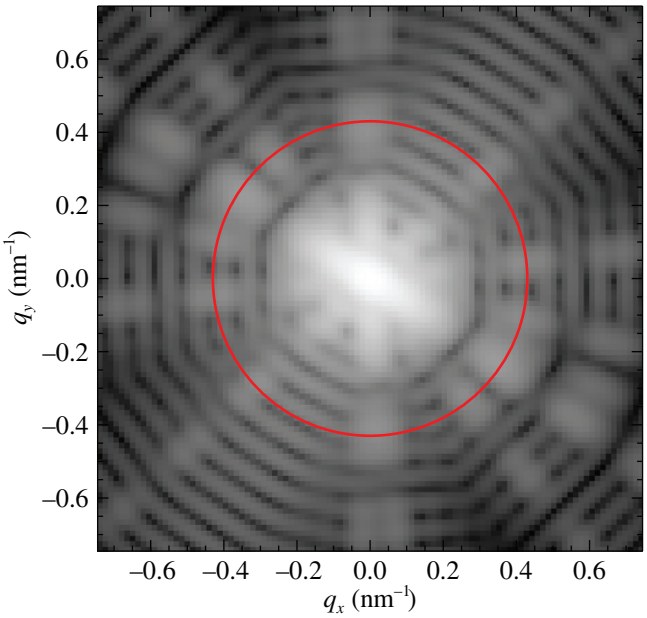

Figure 2. Typical simulated diffraction pattern from ten randomly positioned rods, randomly oriented about an axis parallel to the incident beam. The circle marks the same resolution ring as in figure 1.

4. Circular harmonic expansion and angular correlation functions

We begin by representing the single-particle diffraction pattern (figure 1) by the circular-harmonic expansion

$$I(q_x, q_y) = \sum_m I_m(q) \mathrm{e}^{\mathrm{i}m\phi}, \tag{2}$$

where $I(q_x, q_y)$ represents the intensity of a point on the diffraction pattern of Cartesian reciprocal-space coordinates (q_x, q_y) or equivalent polar coordinates (q, ϕ). In general, the coefficients $I_m(q)$ are complex valued. It should be noted that since the circular harmonics $\mathrm{e}^{\mathrm{i}m\phi}$ form a complete orthonormal set of basis functions for the expansion of an arbitrary intensity distribution around a resolution ring of magnitude q, the set of coefficients $I_m(q)$ for appropriately spaced resolution rings, q, can represent any planar diffraction pattern. The reality of $I(\mathbf{q})$ dictates that $I_{-m}(q) = [I_m(q)]^*$. If the scattering angles are small enough that a flat Ewald sphere may be assumed, Friedel's rule $I(-\mathbf{q}) = I(\mathbf{q})$ implies that only even values of m are nonzero in the sum on the rhs of (2).

Angular pair-correlation functions spanning pairs of resolution rings specified by q and q' are calculated in two steps. First, the data $I(q, \phi)$ of each resolution ring q are mean subtracted to find

$$I'(q, \phi) = I(q, \phi) - \langle I(q, \phi) \rangle_\phi. \tag{3}$$

For small values of q, $\langle I(q, \phi) \rangle_\phi$ may be identified with the usual SAXS signal $I_{\mathrm{SAXS}}(q)$. We then define an angular pair correlation taken between the data on two resolution rings of radii q

and q' of a diffraction pattern by the following equation [7, 8, 10]:

$$C_2(q, q', \Delta\phi) = \frac{1}{N_\phi} \sum_{\phi} I'(q, \phi) I'(q', \phi + \Delta\phi). \tag{4}$$

Likewise, one may define a triple correlation [12] over the resolution ring q by

$$C_3(q, q, \Delta\phi) = \frac{1}{N_\phi} \sum_{\phi} [I'(q, \phi)]^2 I'(q, \phi + \Delta\phi). \tag{5}$$

Their angular discrete Fourier transforms are defined by

$$B_m(q, q') = \frac{1}{N_\phi} \sum_{\Delta\phi} C_2(q, q', \Delta\phi) \mathrm{e}^{-\mathrm{i}m\Delta\phi} \tag{6}$$

and

$$T_m(q, q) = \frac{1}{N_\phi} \sum_{\Delta\phi} C_3(q, q, \Delta\phi) \mathrm{e}^{-\mathrm{i}m\Delta\phi}. \tag{7}$$

5. Algorithm for recovering a single-particle diffraction pattern from multi-particle ones

Correlation functions of the form C_2 and C_3 would be expected to be identical regardless of the orientation of a particle about an axis parallel to the incident radiation [13]. If multiple particles, randomly oriented about this axis, scatter incident radiation under conditions where interparticle interference is negligible, the resulting diffraction pattern would be a superposition of those of the individual particles, and thus C_2 and C_3 calculated from this composite diffraction pattern and averaged over many such diffraction patterns (we included data from 100 such simulated patterns) would be expected to converge on the corresponding quantities for a single particle. We may write

$$I'(q, \phi) = \sum_j \sum_{m \neq 0} I_m(q) \mathrm{e}^{\mathrm{i}m(\phi - \eta_j)} \tag{8}$$

where the subtraction of $\langle I(q, \phi) \rangle_\phi$ in (3) is equivalent to omitting the term $m = 0$ in this summation and where η_j is the (random) orientation of particle j about $\hat{z}$.

Substituting (8) into (6) and (7), it may be shown that

$$B_m(q, q') = N_\mathrm{p} I_m(q) I_m^*(q') \quad \text{for } m \neq 0, \tag{9}$$

where N_p is the number of particles illuminated, and that

$$T_m(q, q) = N_\mathrm{p} I_m^*(q) \sum_{M \neq 0, m} I_M(q) I_{m-M}(q) \quad \text{for } m \neq 0. \tag{10}$$

The quantities on the lhs of (9) and (10) may be found from the angular Fourier transforms of pair- and triple-correlation functions computable from measured data of diffraction patterns from multiple particles. Since this is a quantity from measurement, and the quantities from the rhs are from theory, and since we seek only relative magnitudes of the circular-harmonic expansion coefficients, $I_m(q)$, we could simply remove the common scaling factor, N_p, from equations (6) and (10) and estimate

$$|I_m(q)| = \sqrt{B_m(q, q)} \quad \text{for } m \neq 0 \tag{11}$$

($B_m(q,q)$ is real and non-negative from (9)). A full determination of these expansion coefficients requires also an estimation of the phases of $I_m(q)$.

From (9), with the factor of N_p omitted,

$$I_m(q) = B_m(q,q')/I_m^*(q') \quad \text{for } m \neq 0. \tag{12}$$

Thus, the determination of the phase of I_m for a single resolution ring (say q') uniquely determines the phases of I_m for the same value of m for all other rings q'.

Indeed, substitution of (12) into (10) (with N_p omitted) leads to

$$T_m(q,q) = \frac{B_m^*(q,q')}{|I_m(q')|\mathrm{e}^{\mathrm{i}\phi'(m,q')}} \sum_{M\neq 0,m} \frac{B_M(q,q')}{|I_M(q')|\mathrm{e}^{-\mathrm{i}\phi'(M,q')}} \frac{B_{m-M}(q,q')}{|I_{m-M}(q')|\mathrm{e}^{-\mathrm{i}\phi'(m-M,q')}}, \tag{13}$$

for $m \neq 0$. The only unknowns in (13) are the (real) phases $\phi'(M,q')$ of the circular-harmonic expansion coefficients, $I_M(q')$, for $M \neq 0$.

Once again, the quantity on the lhs of (13) may be found from experiment. In general, there are μ unknown phases $\phi'(M,q')$ *for a single resolution ring* q', where μ is the number of values of M that give rise to distinct values of $I_M(q')$. In our simulation, we took circular-harmonic expansion coefficients M up to a maximum value 38; hence given the fact that $I_{-M}^*(q) = I_M(q)$ and that M takes up only even values, $\mu = 19$. In general, these μ real numbers may be found by optimizing the function

$$\sum_{m\neq 0} |T_m^{(\mathrm{obs})} - T_m^{(\mathrm{calc})}|^2 \tag{14}$$

by means of a global optimization algorithm such as simulated annealing [14] (where $T_m^{(\mathrm{obs})}$ are the quantities found from the angular Fourier transforms of the triple correlations C_3 from the measured diffraction patterns, and $T_m^{(\mathrm{calc})}$ their values estimated from the rhs of (13)). In the present simulation, for an individual object that gives rise to a diffraction pattern with a mirror line, the origin of the angular coordinate may be taken about this line and the coefficients $I_M(q)$ taken to be real. Then, the only uncertainties are their signs. In this case, even an exhaustive search through 2^{19} sign combinations to optimize (14) took no more than a few minutes on a laptop computer. The value of $I_0(q)$ is estimated from the same data via $\langle I(q,\phi)\rangle_\phi$, the angular average of the intensities of resolution rings q. (Since $I_0(q)$ is real and positive, there is no need to determine *its* phase (or sign).)

6. Simulations

The importance of the determination of the phases $\phi'(m,q')$ (or in this case, the signs $s(m,q')$) via the triple correlations C_3 and (13) may be judged by the diffraction pattern (figure 3) simulated via (2) with the magnitudes of $I_m(q)$ determined by (11) and random independent signs and (2). This is seen to bear no relation whatsoever to the simulated single-particle diffraction pattern of figure 1.

The step of determining the signs of $I_m(q)$ via the angular triple correlations is crucial, as the reconstructed pattern bears no relation to even the central part of figure 1 for random signs of $I_m(q)$.

The result of reconstructing the single-particle diffraction pattern up to the resolution ring marked in figure 1 with the quantities $I_m(q)$ from the correlations C_2 and C_3 and SAXS data of 100 multi-particle diffraction patterns like figure 2 are shown in figure 4. A remarkable

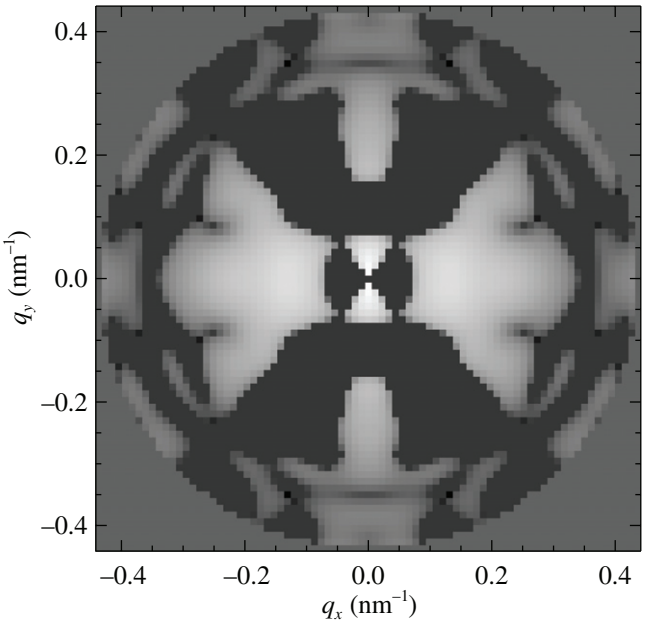

Figure 3. Part of the single-particle diffraction pattern within the red resolution ring of figure 1 reconstructed from the magnitudes $|I_m(q)|$ of the circular-harmonic expansion coefficients determined from the pair correlations C_2 and random signs of the coefficients.

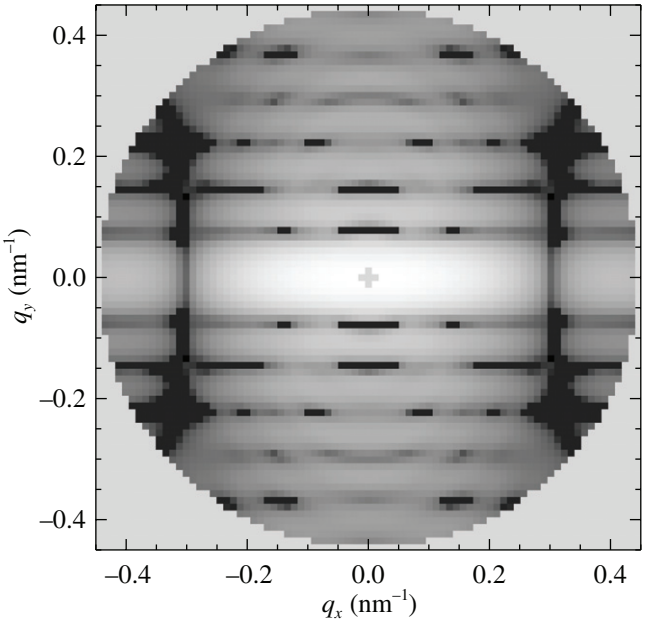

Figure 4. Single-particle diffraction pattern within the red ring of figure 1 reconstructed from the magnitudes of $I_m(q)$ determined from the mean pair correlations C_2, and signs from the mean triple correlations C_3 from 100 multi-particle diffraction patterns like that of figure 2.

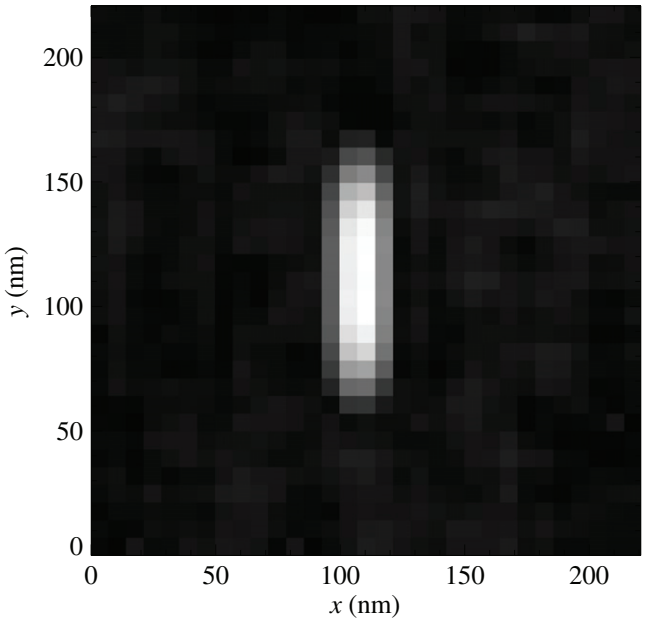

Figure 5. Real-space image of the 80 nm × 25 nm projection of the cylindrical object recovered to ∼ 7 nm resolution from the reconstructed single-particle diffraction pattern of figure 4 after ∼15 iterations of the charge-flipping algorithm [14].

similarity to the model single-particle diffraction pattern of figure 1 is apparent. Simulated Poisson noise produces an unimportant peak at the origin of the correlation functions C_2 and C_3. For the parameters of our simulations, interference fringes from interparticle interference are finer than a detector pixel, and are thus irrelevant.

7. Reconstruction of the projected electron density of a single rod from the recovered single-particle diffraction pattern

Finally, we recover (figure 5) from the diffraction pattern of figure 4 the projected electron density of the individual particle, after ∼ 15 iterations of the *charge-flipping* algorithm [15]. An unambiguous reconstruction of the 80 nm × 25 nm rod projection to the resolution of the reconstructed diffraction pattern ($\sim \pi/0.45 \simeq 7$ nm) is found, without any assumption about compact support of the particle. The fidelity of the reconstruction may be judged by the fact that in the direction of the rod diameter (the short direction of the projected electron density, parallel to the x-axis) even a tapering off of the electron density towards the edge is seen, exactly as expected for the projection of a solid cylinder.

8. Experimental

In order to test these ideas, we have collected soft x-ray transmission diffraction patterns at the Advanced Light Source (ALS) from gold nanorods ($25 \times 80\,\text{nm}^2$) lying on their side on a transparent silicon nitride membrane. To prepare individual isolated gold nanorods

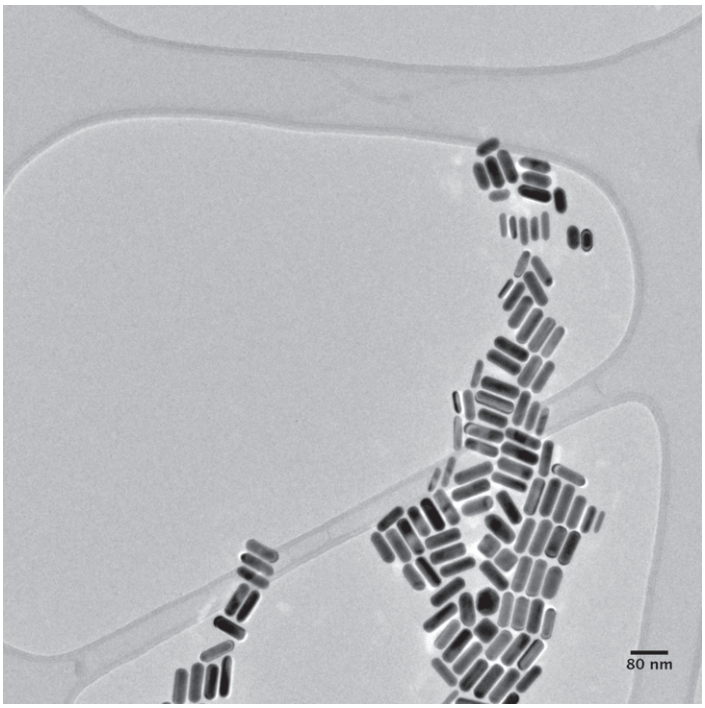

Figure 6. TEM image of gold nanorods, 25 nm × 80 nm^2 in projection, lying on an SiN membrane of 100 nm thickness. In the scattering experiment whose results are reported here, the rods were not clumped, as shown here, but dispersed to be randomly oriented, with random interparticle distances.

on the surface, a solution of nanorods was aerosolized via charge-reduced electrospray and electrostatically captured onto the silicon nitride membrane using previously described methods [11].

Figure 6 shows a transmission electron microscope (TEM) image of these rods, which differ only by rotation about the normal to the membrane. Rotation of one rod about the beam direction therefore rotates its diffraction pattern by the same amount. Using 750 eV highly coherent x-rays (1.65 nm wavelength), hundreds of diffraction patterns were collected from different 15 μm-diameter regions, each containing 20–100 rods. In these patterns, the distance between rods is so large that coherent interference fringes resulting from different particles are much finer than the features from individual rods. The resulting patterns were analyzed by dividing the patterns into annular rings and forming the ring autocorrelation (RAC) functions defined in equation (4) with $q' = q$. We may now test the hypothesis that the sum of many such rings for a given q over many patterns converges to the RAC functions for a single rod, using these experimental data. If so, the retrieval of a real-space image of one rod requires only solution of the phase problem twice: firstly, to recover the diffracted intensity from its RAC functions, and secondly, to recover the object charge-density from its diffraction pattern intensity distribution.

Figure 7 shows a typical diffraction pattern with the path of a ring indicated at L. The resolution of this ring at q is about 34 nm. Figures 8 and 9 show RAC functions computed around this path, with the abscissa range from 0 to 180°. Figure 8 shows the result for the first RAC (lower panel, dashed line), obtained from a diffraction pattern, which includes tens

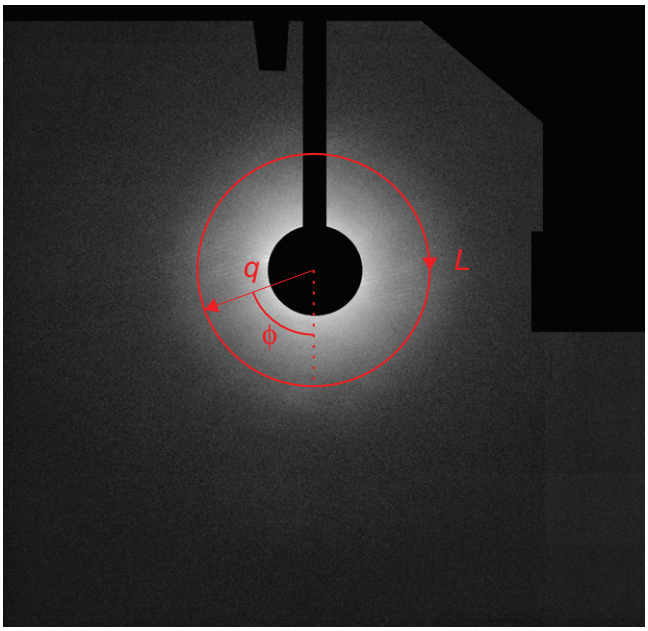

Figure 7. Typical soft x-ray (750 eV) transmission diffraction pattern from groups of rods shown in figure 6. The pattern shows fluctuations from the typical isotropic 'SAXS' form because they are stationary and few. The intensities shown in figure 8 are plotted around a ring such as L at q.

of randomly oriented rods. The continuous line (lower panel) shows a simulation of the RAC function for a single rod. The upper panel shows the intensity in the diffraction pattern plotted using a logarithmic intensity scale. In figure 9, 121 of these RAC functions (from different regions of the sample) have been summed, and the result is compared again with the simulated RAC function from a single rod (lower panel). The experimental sum is seen to converge well to the model curve.

During these many hours of automated data recording (with computer-controlled sample stage motions for each new region) the intensity of the x-ray source steadily decreased.

9. Discussion and conclusions

Although demonstrated in this paper only for an artificial object of rectangular projection, these results suggest the possibility of deducing the diffraction pattern of a single particle from the angular correlations of a diffraction pattern from the scattering of radiation from multiple identical particles in random orientations. If this were possible, it should also be possible to reconstruct an image of an individual particle via an iterative phasing algorithm applied to an oversampled reconstructed single-particle diffraction pattern.

Such a demonstration opens up the possibility for the following future extensions:

1. The generalization of this method to particles of no particular projected symmetry, such as a general protein molecule.
2. An application [12] to particles entirely randomly oriented in three dimensions (3D), allowing the structure determination of a difficult-to-crystallize molecule from short-pulse

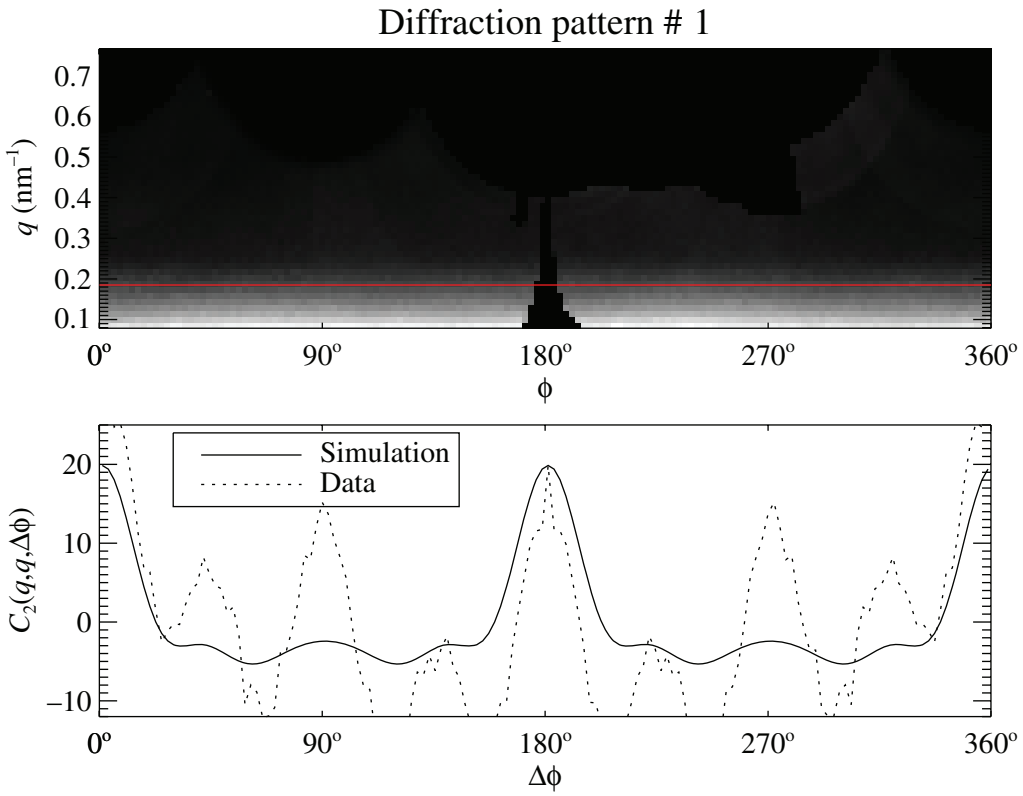

Figure 8. Upper panel: diffracted intensity from a single x-ray diffraction pattern from a group of rods in random orientations. The ring L of figure 7 is represented by the red horizontal line in this plot, in which the diffraction pattern intensities are plotted on a logarithmic gray scale, with brighter regions representing higher intensities. The dark 'finger' around $\phi = 180^\circ$ is a projection of the beamstop holder (see figure 7). Lower panel: RAC function (dotted curve) from the experimental diffraction pattern of the upper panel and from a simulated diffraction pattern of a single rod (continuous curve).

diffraction patterns of such molecules in solution, provided that scattering by solution atoms may be minimized or isolated.

3. The results are relevant also to the kind of 'diffract and destroy' approach to biomolecular structure determination [16] proposed for the x-ray free electron laser (XFEL), where measurements of diffraction from single molecules have been proposed. In this case, the SAXS background, which arises from uncorrelated scattering by *different* particles, is entirely absent, as is scattering from solution atoms [8]. Alternatively, the ability to extract meaningful information from multi-particle diffraction patterns may help overcome intensity issues from single-particle scattering.
4. The method is not restricted to diffraction patterns from scattering of externally incident radiation. A diffraction pattern may be measured also from x-rays arising from the fluorescence of a specific atom buried deeply within a large molecule [17] (e.g. the Fe atom in hemoglobin). Such a pattern would be most sensitive to intramolecular scattering,

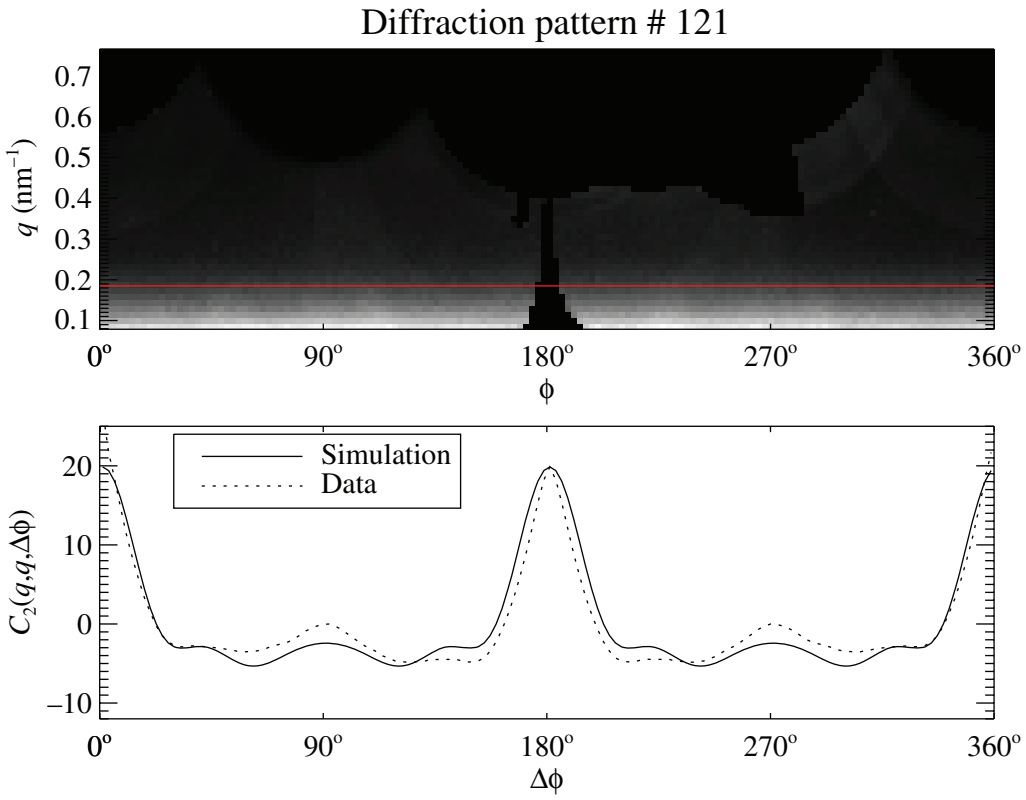

Figure 9. Upper panel: intensity of diffraction pattern no. 121, plotted as in figure 8. Lower panel: average RAC function from the data of many such diffraction patterns (dotted line). This is seen to approximate well to the corresponding calculated RAC function for a single rod.

less to that from its surroundings. This may allow the reconstruction of the 3D diffraction volume of an individual molecule from that of many randomly oriented ones and hence of the molecular structure, without too much interference from solvent (or membrane) scattering.

Advances in technology, such as fast column read-out area detectors, brighter sources, shorter pulses and zone-plate focusing, have greatly improved the experimental conditions for such experiments. When coupled with new theoretical advances, such as those reported here, entirely new vistas are opened up for the structure determination of microscopic particles.

Acknowledgments

DKS and JCHS jointly acknowledge support for the present work from the US Department of Energy (DOE) grant DE-SC0002141, UW, KES and JCHS from NSF grant MCB-0919195, DKS from DE-FG02-06-ER46277 and the UWM Research Growth Initiative and JCHS from DE-FG03-02ER45996 and the NSF Center for Biophotonics Science and Technology. Part of the work was funded by the DOE at the SLAC National Accelerator Laboratory under contract number DE-AC02-76F00515. The Lawrence Berkeley National Laboratory and Advanced

Light Source facility are supported by the Director, Office of Energy Research, Office of Basic Energy Sciences, Materials Sciences Division of the DOE, under contract no. DE-AC03-76SF00098.

References

[1] Elser V and Millane R P 2008 *Acta Crystallogr.* A **64** 273
[2] Howells M R *et al* 2009 *J. Electron Spectrosc. Relat. Phenom.* **170** 4
[3] Marchesini S 2007 *Rev. Sci. Instrum.* **78** 049901
[4] Stuhrmann H B 1970 *Acta Crystallogr.* A **26** 297
[5] Svergun D I and Stuhrmann H B 1991 *Acta Crystallogr.* A **47** 736
[6] Svergun D I and Koch M H 2002 *Curr. Opin. Struct. Biol.* **12** 654
[7] Kam Z 1977 *Macromolecules* **10** 927
[8] Saldin D K, Shnerson V L, Fung R and Ourmazd A 2009 *J. Phys.: Condens. Matter* **21** 134014
[9] Doyle D A, Cabral J M, Pleutzner R A, Kuo A, Gulbis J M, Cohen S L, Chait B T and MacKinnon R 1998 *Science* **280** 69
[10] Wochner P, Gutt C, Autenrieth T, Demmer T, Bugaev V, Ortiz A D, Duri A, Zontone F, Grübel G and Dosch H 2009 *Proc. Natl Acad. Sci. USA* **106** 11511
[11] Bogan M J, Benner W H, Hau-Riege S P, Chapman H N and Frank M 2007 *J. Aerosol Sci.* **38** 1119
[12] Kam Z 1980 *J. Theor. Biol.* **82** 15
[13] Kam Z 1982 *Uses of Synchroton Radiation in Biology* ed H B Stuhrmann (London: Academic)
[14] Kirkpatrick S, Gelatt C D and Vecchi M P 1983 *Science* **220** 671
[15] Oszlányi G and Sütó A 2004 *Acta Crystallogr.* A **60** 134
[16] Neutze R, Wouts R, van der Spoel D, Weckert E and Hajdu J 2000 *Nature* **406** 752
[17] Faigel G, Bortel G, Fadley C S, Simionovici A S and Tegze M 2007 *X-Ray Spectrom.* **36** 3